HELICoiD Demonstrator for Intraoperative Brain Cancer Detection using Hyperspectral Images

Himar Fabelo, Gustavo M. Callicó, Aurelio Vega,
Minerva Alemán, Adrian de Pablo, Roberto Sarmiento
Institute for Applied Microelectronics (IUMA)
University of Las Palmas de Gran Canaria (ULPGC)
Las Palmas de Gran Canaria (Spain)
{hfabelo, gustavo, avega, maleman, apablo,
roberto}@iuma.ulpgc.es

Lucas Sanjuán
ONCOVISION, GEM-IMAGING S.A.
Centro de Investigación Príncipe Felipe
Valencia (Spain)
lucas.sanjuan@oncovision.com

Abstract—**This paper describes the process carried out for the developing of a demonstrator within the HELICoiD (HypErspectraL Imaging Cancer Detection) European project, in order to achieve a system capable to discriminate, with high precision, between healthy and tumour tissues in neurosurgical operations. The HELICoiD demonstrator is composed by two hyperspectral cameras and an illumination system that cover the spectral range from 400 nm to 1700 nm. A data processing unit is in charge of managing all the parts of the demonstrator, and a high performance platform aims to accelerate the hyperspectral image processing. Each one of this elements are installed in a customized structure specially design for surgical environments. This intraoperative system can help neurosurgeons in the brain tumour resection, avoiding the excessive extraction of healthy tissue thanks to the high accuracy of the system to detect the borders of the tumour and avoiding accidental leaving of small tumour tissues. The results are provided by the hyperspectral image classification algorithms in real time, allowing a precise discrimination between healthy and tumour tissues.**

Keywords—hyperspectral imaging; brain cancer detection; medical systems.

I. INTRODUCTION

Brain cancer is one of the most important forms of the disease. The most common form is high-grade malignant glioma, which accounts for approximately 30-50% of primary brain cancers, with multiform glioblastoma making up 85% of these cases. These types of gliomas are characterized by fast-growing invasiveness, which is locally very aggressive, are in most cases unicentric and are rarely metastasizing.

Traditional diagnoses of internal tumours are based on excisional biopsy followed by histology or cytology. The main weakness of this standard methodology is twofold: firstly, it is an aggressive and invasive diagnosis with potential side effects and complications due to the surgical resection of both, malign and healthy tissues; and secondly, diagnostic information is not available in real time and needs the tissues being processed in a laboratory. The importance of complete resection for low grade tumours has been discussed and it has proven to be beneficial, especially in paediatric cases.

Currently, there are several alternatives to traditional optical imaging technology, being the most outstanding one the magnetic resonance imaging (MRI), the computed tomography (CT), the ultrasonography, the Doppler scanning and the nuclear imaging. Hyperspectral imaging arises as a potential solution that allows a precise detection of the edges of the malign tissues in surgical time, while assisting guidance for diagnosis during surgical interventions and treatment [1][2].

Hyperspectral imaging is a non-contact, non-ionizing and minimal-invasive sensing technique suitable for medicine. It consists in collecting and processing information from across the electromagnetic spectrum. It increases the information content acquired from a scene, compared with a conventional or a multi-spectral image, by capturing data in a large number of contiguous and narrow spectral bands over a wide spectral range. With that information it is possible to obtain a spectral signature of each pixel. This spectral signature allows differentiating the material or substance that is presented in the pixel. As cancer involves changes in the cellular physiology, it should be detected as a change in the hyperspectral signature of the tissue. Using the hyperspectral signatures of healthy tissue and the same tissue affected by cancer, a model of how cancer affects the signature could be derived. Fig. 1 shows the spectral signatures obtained with a spectrograph from a tumour and healthy pathology samples [3].

Hyperspectral imaging has been used in diverse medical studies, showing that this technique is able to capture images of a large area of tissue and has exhibited great potential in the diagnosis of cancer in cervix, breast, colon, gastrointestine, skin, ovary, urothelial carcinoma, prostate, esophagea, trachea, oral tissue, tongue and lymph node [4]-[8]. However, hyperspectral imaging systems are not standardised, as different technologies have been used in these studies.
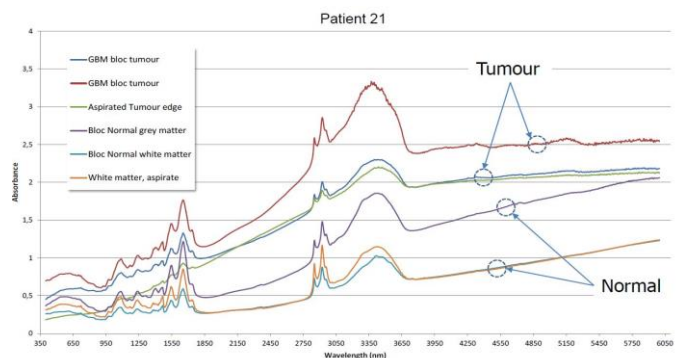

Fig. 1. Spectral signatures of tumour and healthy tissues from spectrographic samples.

Hyperspectral cameras generally use a CCD detector, which have an average spectral resolution of 5 nm and normally have a spectral range of 600 nm, from 400 nm to 1200 nm or larger. As a result, in some cases two devices (visible-to-near-infrared and near-infrared cameras) are used to achieve the required range, as it is done in the creation of library of spectral signatures for abdominal organs, arteries and veins [9], or in the study of detection and analysis of intestinal ischemia during surgeries [10]. Regarding to the illumination systems used with the cameras, they consist mainly in halogen or xenon lamps, and sometimes optic fibre is used for light transmission, like in the diffuse reflectance spectroscopy used for early detection of malignant changes in the oral cavity [11]. High performance acquisition computers were needed to be able to work with large data hyperspectral images, like the Intel CPU i7 with 4GB RAM used to measure and analyse the reflectance spectra of the human tongue [12].

Although there is no antecedent in the use of hyperspectral imaging in brain surgeries, one of the major benefits from this technology, could be the accuracy in removal of brain tumours. Unlike other tumours, brain tumours infiltrate the surrounding tissue and thus their borders are indistinct and difficult to identify. The surrounding brain tissue is critical and there is no redundancy as is seen in many other organs where it is normal to remove the tumour together with a surrounding rim of healthy tissue. This is not possible in the brain where it is essential to identify accurately the border between normal and diseased tissue. As a result, hyperspectral imaging techniques can be applied for a precise localization of malignant tumours during surgical procedures.

The HELICoiD project is a European collaborative project funded by the Research Executive Agency, under Grant Agreement 618080, through the Future and Emerging Technologies (FET-Open) programme, under the 7th Framework Programme of the European Union. The project is a collaboration between four universities, three industrial partners and two hospitals.

The main goal of the project is to use hyperspectral imaging to generalize the methodology to discriminate between healthy and malignant tissues in real-time during surgical procedures. This information will be provided to the surgeon in real time via different display devices, and in particular by overlaying the conventional images with a simulated colour map which indicates the healthy tissues and the tissues affected by tumour cells. The integration of hyperspectral imaging and intraoperative imaged guided surgery systems should have a direct impact on patient outcomes. Potential benefits include: allowing confirmation of complete resection during the surgical procedure, avoiding complications due to "body mass shift", and providing confidence that the goals of the surgery have been achieved.

In order to reach this goal, the HELICoiD project has developed an experimental intraoperative demonstrator based on two non-invasive hyperspectral cameras that covers the wavelength range of 400 nm to 1700 nm. This system is described in the remainder sections of this paper.

II. HELICoiD Demonstrator

This section provides an overview of the demonstrator for intraoperative brain cancer detection developed in the HELICoiD project. As it can be seen in Fig. 2, the demonstrator is composed by four main parts: the acquisition scanning platform, which is composed by the hyperspectral cameras and the illumination system; the data pre-processing system, where the core software that manages all the system is located; the processing sub-system platform, where the hyperspectral classification algorithms are implemented; and the user interface, where the demonstrator operator controls all the system.
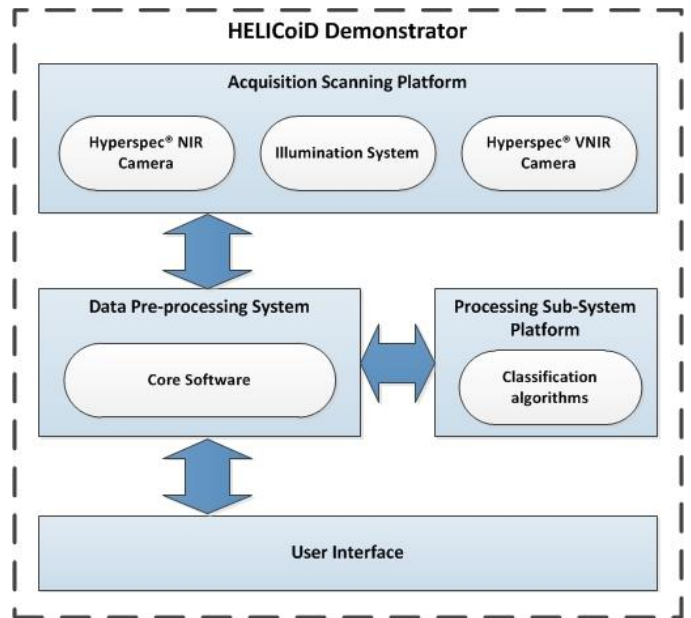

Fig. 2. HELICoiD demonstrator main parts.

A. Acquisition scanning platform

1) Hyperspectral cameras

The hyperspectral cameras selected for the HELICoiD demonstrator are a combination of the cameras Hyperspec® VNIR A-Series and Hyperspec® NIR 100/U (manufactured by HeadWall Photonics, Massachusetts, USA). The main characteristics of these cameras are presented below:

- **The Hyperspec® VNIR A-Series** model has the spectral range of 400 – 1000 nm (visible and near infrared frequency), a dispersion per pixel of 0.74 nm and a spectral resolution of 2 – 3 nm (with a 25 μm slit), being able to capture 826 spectral bands and 1004 spatial bands. This device integrates a Silicon CCD detector array with a minimum frame rate of 90 fps. The lens used in this camera is a Xenoplan 1.4 with 22.5 mm of focal length and a broadband coating for the spectral range of 400 nm to 1000 nm.

- **The Hyperspec® NIR 100/U** model has a spectral range of 900 – 1700 nm (near infrared frequency), a dispersion per pixel of 4.8 nm and a spectral resolution of 5 nm (with a 25 μm slit), being able to capture 172 spectral bands and 320 spatial bands. This system incorporates an Indium Gallium Arsenide (InGaAs)

detector array which provides a fast response, a high quantum efficiency and low dark current for the sensor area. This system allows achieving a frame rate of 100 fps. The lens used in this camera is a Kowa LM25HC-SW 1.4 with 25 mm of focal length and a broadband coating for the spectral range of 800 nm to 2000 nm.

The capturing technique of both cameras is based in a pushbroom scanner. This technique allows the 2-D detector matrix of the camera to capture the spectral dimension and one spatial dimension. By shifting the camera's field of view (FOV) relative to the objet, the second spatial dimension is created. TABLE I. shows the specifications of the used cameras.

TABLE I.　CAMERA SPECIFICATIONS

	Hyperspec® VNIR	Hyperspec® NIR
Spectral range (nm)	400 – 1000	900 – 1700
Spectral resolution (nm)	2 – 3	5
Slit (μm)	25	25
Spatial bands	1004	320
Spectral bands	826	172
Frame Height (FOV) (mm)	129.21	153.6
Pixel Dimensions (IFOV) (mm)	0.1287	0.4800
Max Pixels per Frame	1004	320
Max Frames per Capture	1825	489
Dispersion per pixel (nm)	0.74	4.8
Detector array	Silicon CCD	InGaAs
Frame rate (fps)	90	100
Data interface	Base Camera Link™	USB 2.0

2) Scanning platform

The cameras are installed in a scanning platform in order to provide the movement needed by them. It is a customized unit composed by a stepper motor and a screw (BiSlide® motor-driven assembly) with a maximum path of 235 mm. The BiSlide® system is managed by a Velmex VXM® stepping motor controller. Normally, the scanned objects are moved instead of the hyperspectral cameras. However, in this case is not possible to move the scanned tissue, as this would involve moving the patient and the set of instruments used during the surgery. Consequently, it is necessary to move the cameras and the illumination system to achieve the pushbroom imaging technique which is needed to scan line by line the selected brain tissue area, as it is required by the hyperspectral imaging system proposed. Fig. 3 illustrates the hyperspectral cameras mounted in the scanning platform.
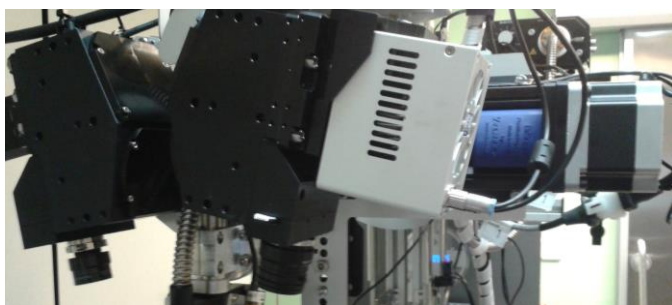

Fig. 3.　Hyperspectral cameras mounted on the scanning platform.

3) Illumination system

The illumination system of the demonstrator is composed by two main parts, the light source and the cold light emitter. The light source is a Techniquip Model 21 DC which consists of a 150 W Quartz Tungsten-Halogen system (QTH). This kind of lamps offers broadband emission in the VIS and NIR spectral ranges (400 nm to 2200 nm), so they are ideal for spectrophotometers. However, it is relevant to mention that QTH lamps generate high temperature in the environment near the bulb and this high temperature can cause damage and even premature death of cells. In this application it is very dangerous and it is necessary to use a fibre-optic to transmit the light to a cold light emitter in order to reduce the temperature of the focusing light. Fig. 4 shows the light source and the cold light emitter located in the scanning platform.
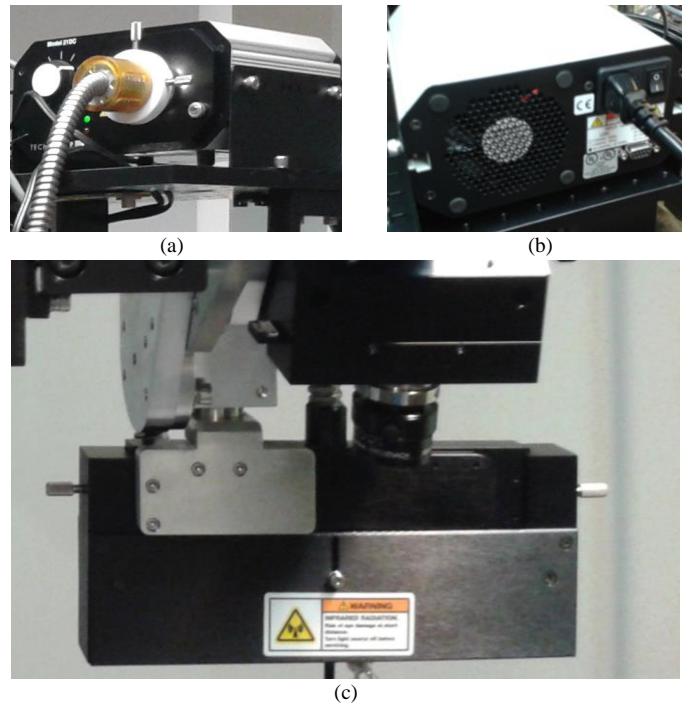

Fig. 4.　(a) Light source front view with the fibre optic connected. (b) Light source rear view. (c) Cold light emitter.

B. Data pre-processing system

The data pre-processing system consists on a Hyperspec® Data Processing Unit (HDPU) (Fig. 5), which is a high speed computer. In this device is installed de core software, which is in charge of manage the cameras and the scanning platform. It has also the aim of pre-processing the hyperspectral images and transmits these pre-processed images to the processing sub-system platform, receives the classification results from it and display these results to the operator through the user interface.

The selected HDPU is a Modified Commercial Off-The-Shelf (MCOTS) system that provides high-speed data processing and storage for many applications, especially for the HELICoiD project. The HDPU is composed by a 3.5 GHz quad-core processor, with 8 GB of RAM and a high-capacity 512 GB solid-state drive with write speeds exceeding 500 MB/s. It supports both Windows and Linux operating systems

and it is pre-loaded with Headwall's Hyperspec III software. This software is able to carry out the tasks related with the management of the cameras and the scanning platform.

Fig. 5. Hyperspec® Data Processing Unit.

C. Processing sub-system platform for algorithms implementation

The HDPU requires a processing sub-system platform for the hyperspectral classification algorithm implementation, due to the complexity of this kind of algorithms and the high amount of data obtained from the hyperspectral images.

Fig. 6 shows the platform selected for this issue which is a Kalray many-core processor that features MIMD (Multiple Instruction Multiple Data) architecture. This platform is focused on compute intensive, low power, embedded applications. Its series of Multi-Purpose Processor Array (MPPA) comprise many 32-bit Very Long Instruction Word (VLIW) cores with floating point unit, grouped in several compute clusters. MPPA 256 processing performance reaches 230 GFLOPS, which, for the 5 W power consumption reported, turns into 46 GFLOPS/W, a much higher figure compared to other kind of high performance platforms.

Fig. 6. Kalray MPPA-256 Board.

D. System interconnection

1) Demonstrator physical interfaces

The HDPU is in charge of interconnecting all the devices that constitute the HELICoiD demonstrator. The VNIR camera is connected to the HDPU using the standard CameraLink interface. This interface provides a data transmission rate up to 255 MB/s. It is required due to the high amount of data generated by the VNIR camera, which can reach up to 6 GB. The NIR camera is connected to the HDPU using a USB 2.0 interface, since, in this case, the transfer rate is up to 60 MB/s, and a NIR image can reach up to 150 MB. In addition, the HDPU is linked to the camera scanning platform using a RS-232 protocol. Finally, the processing sub-system platform is connected to the HDPU through a PCIe 3.0 interface in order to achieve the highest transfer speed.

The HELICoiD demonstrator is controlled basically through medical grade computer peripherals, a keyboard and a mouse as input devices, and a monitor as output device connected through a HDMI (High-Definition Multimedia Interface) port to the HDPU.

2) Demonstrator software interconnection

Fig. 7 represents the core software of the hyperspectral demonstrator, the connections between its modules and the interfaces used for this purpose.
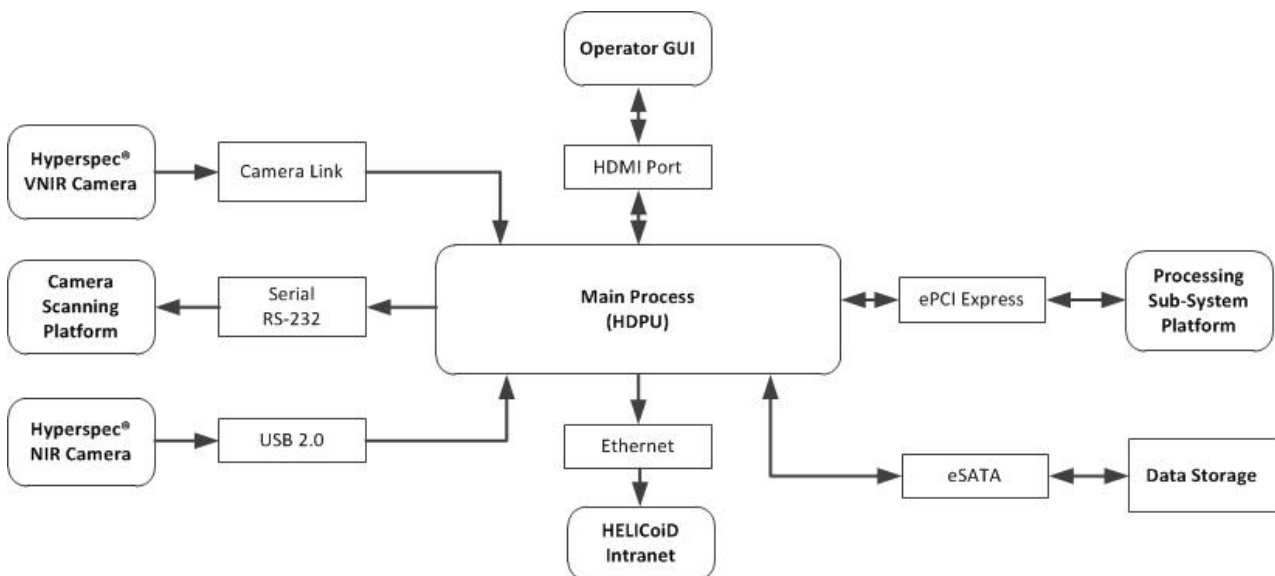

Fig. 7. HELICoiD demonstrator software diagram.

The hyperspectral data cubes obtained with the hyperspectral cameras are sent to the main process. This main process sends signals to move the camera scanning platform and manages the pre-processing of the hyperspectral data cubes. Next, the hyperspectral images are stored in a solid-state drive, and the pre-processed images are sent to the sub-system platform in order to be processed by the hyperspectral classification algorithms. When the images have been processed, the results go back to the main process and they are sent to the operator's Graphical User Interface (GUI). The operator's GUI shows the result of the classification process and also allows controlling the different parameters for the configuration of all process. Finally, the main process is connected to the HELICoiD intranet database, through the Ethernet interface, in order to store the information about the captured brain tissues samples.

E. Final demonstrator

All parts described in the previous point compose the HELICoiD demonstrator. Fig. 8 represents a scheme of the complete structure system and the degrees of freedom obtained by the use of two additional motors for this purpose.
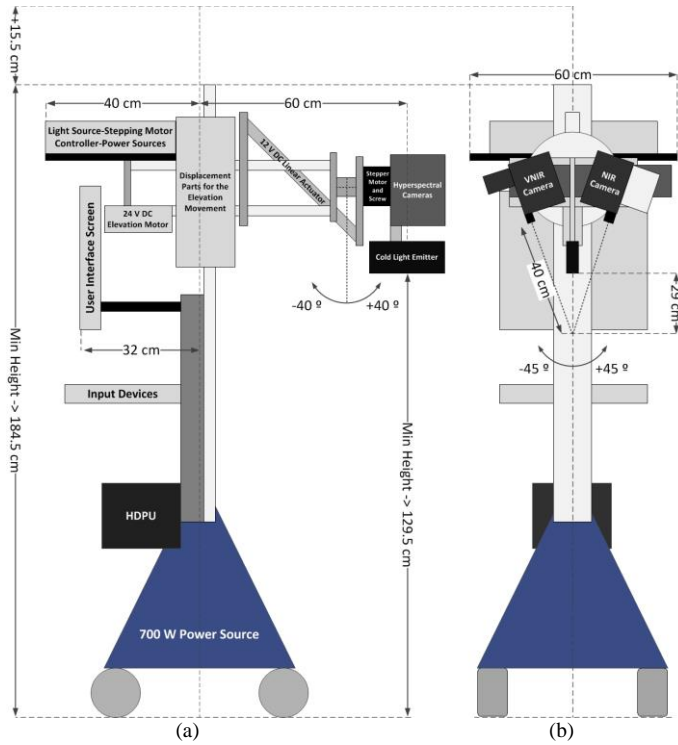

Fig. 8. HELICoiD demonstrator scheme. (a) Side view. (b) Front view.

The movement in the Y-axis is the main movement required for the focus of the camera. This is an important issue since if the images are not well focused, the spectral signature of each pixel will be wrong. The approximate distance between the brain tissue and the lens of the cameras is 40 cm. A 24 VDC motor with a screw is used for this purpose allowing a displacement of ±7.75 cm. The structure also permits rotate the camera scanning platform 40º forward and backward. This movement is done by a 12 VDC linear actuator. Finally, an aluminium plate allows the rotation movement manually, 45º to the left and 45º to the right, as it can be seen in the front view of Fig. 8 (b).

The developed structure allows having a distance between the head of the patient and the mast of the demonstrator of 40 cm approximately. Fig. 9 shows the final HELICoiD demonstrator completely built and Fig. 10 presents the HELICoiD demonstrator being used in the neurosurgical operating theatre at the University Hospital Dr. Negrín of Las Palmas de Gran Canaria.
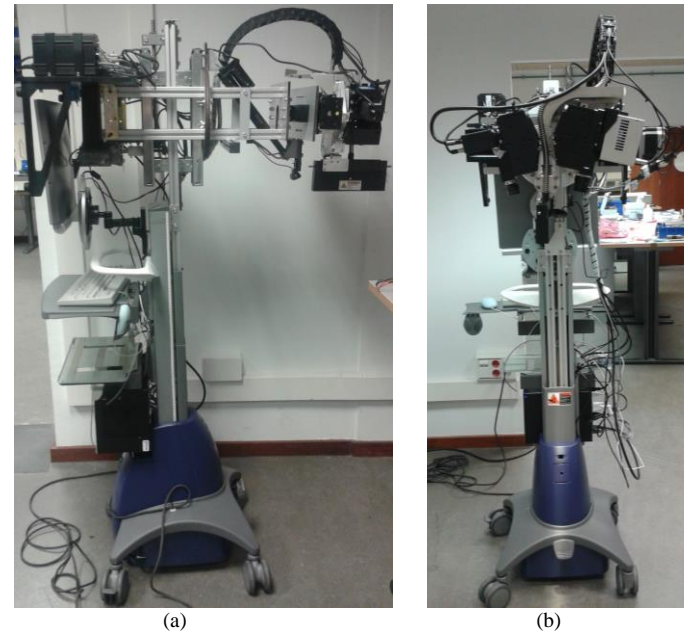

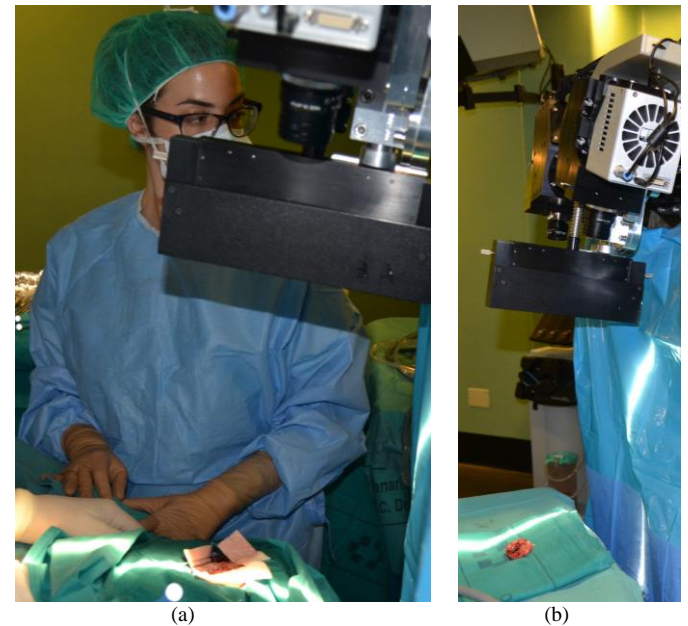Fig. 9. Final HELICoiD demonstrator. (a) Side view. (b) Front view.

Fig. 10. HELICoiD demonstrator in the neurosurgical operating theatre at the University Hospital Dr. Negrín of Las Palmas de Gran Canaria. (a) HELICoiD demonstrator over a patient. (b) HELICoiD demosntrator over a ex-vivo tumour sample.

III. Preliminary Results

A. Brain tumour hyperspectral images

The HELICoiD demonstrator can obtain two hyperspectral data cubes when the acquisition process is executed, one with the VNIR camera and another one with the NIR camera. The VNIR hyperspectral data cube has a height of 1004 pixels (that cover a dimension of 129.21 mm) and each pixel has a dimension of 0.1287 mm x 0.1287 mm. The width of the image will depend on the number of lines that is specified in the software (also in the NIR camera). The maximum number of lines that can be captured with the VNIR camera is 1825 (that cover a dimension of 234.88 mm). The number of spectral bands of this data cube is 826. The NIR hyperspectral data cube has a height of 320 pixels (that cover a dimension of 153.60 mm) and each pixel has a dimension of 0.48 mm x 0.48 mm. The maximum number of lines that can be captured with the VNIR camera is 489 (that cover a dimension of 234.72 mm) and the number of spectral bands is 172.

Fig. 11 and Fig. 12 show some of the most representative bands of a VNIR image and a NIR image respectively of a brain tumour captured in the operating theatre at the University Hospital Dr. Negrín.

B. Preliminary spectral signatures

A pre-processing chain has been applied to the hyperspectral images obtained by the HELICoiD demonstrator in order to homogenise the spectral signatures of each pixel. Fig. 13 represents the different steps of this pre-processing chain. The most important one is the image calibration, where the significant signal variations caused by the non-uniform illumination over the surface of the captured scene is corrected. The acquired raw image is calibrated using the white and dark reference images. White and dark reference images are acquired by the demonstrator with the VNIR and NIR cameras separately, but in the same illumination conditions inside the operating theatre. The white reference image is acquired using a standard white reference tile (Fig. 14) and the dark reference image is obtained by keeping the camera shutter closed. The hyperspectral calibrated image is calculated by the equation (1), where β is the calibrated image, α is the raw image and γ and δ are the white and dark reference images respectively.

$$\beta = 100 \cdot \frac{\alpha - \delta}{\gamma - \delta} \tag{1}$$
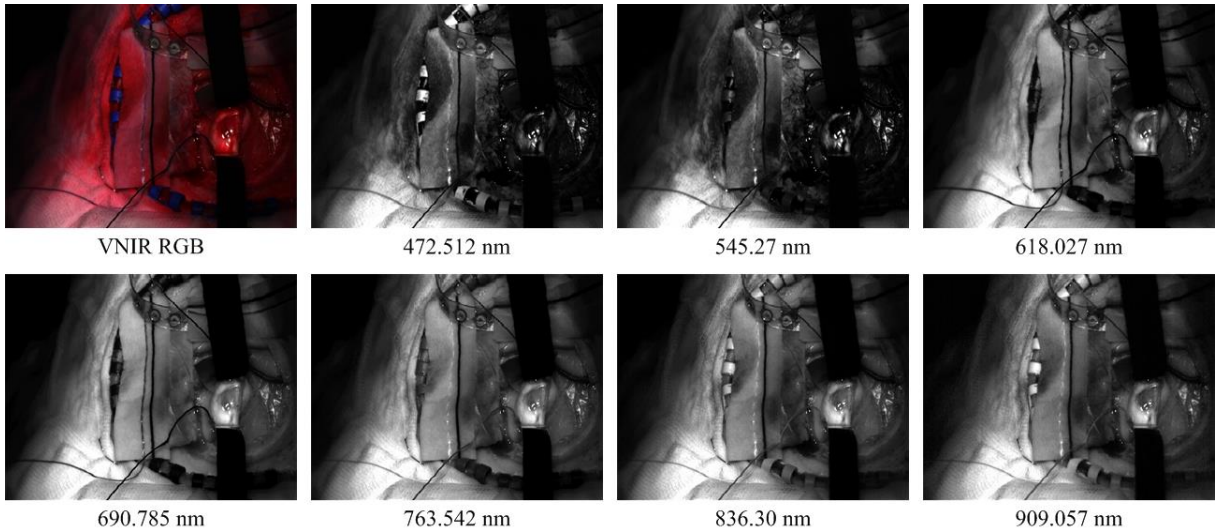

Fig. 11. Most representative bands of the VNIR hyperspectral image (400 nm to 1000 nm).
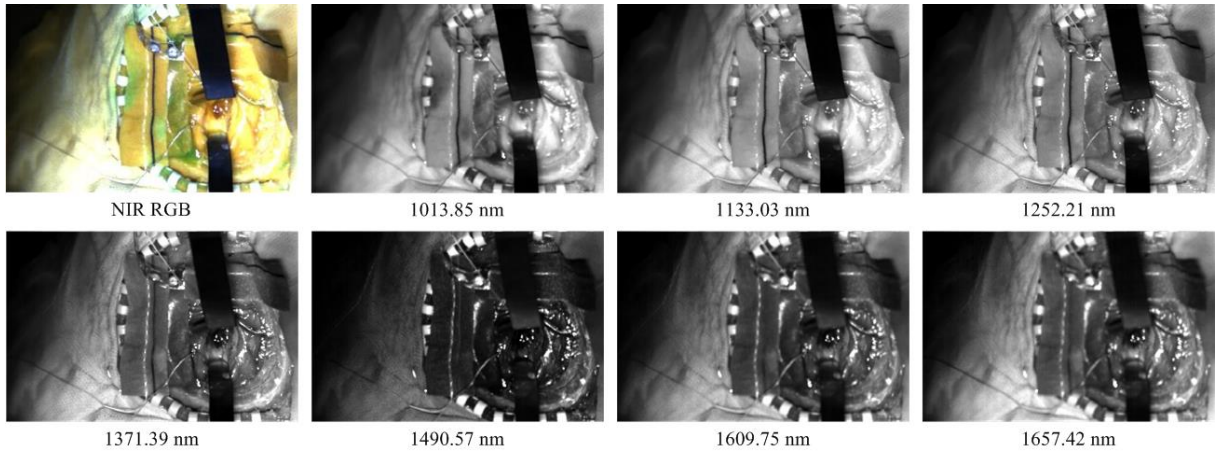

Fig. 12. Most representative bands of the NIR hyperspectral image (900 nm to 1700 nm).
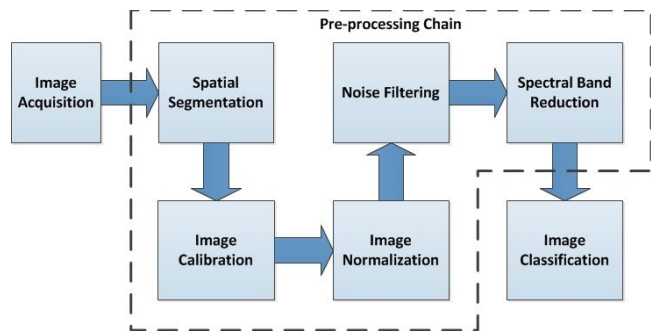
Fig. 13. HELICoiD demonstrator preliminary pre-processing chain.

Fig. 14. White reference tile.

Fig. 15 illustrates the average spectral signatures of 391 healthy pixel samples and 496 tumour pixel samples and their respective minimum and maximum variances. The spectral signatures have been obtained after the application of a basic pre-processing chain without spectral band reduction. As it can be observed, the most relevant spectral range useful for the discrimination between tumour samples and healthy samples is the region among 450 nm to 850 nm. The first and last bands of the image should be rejected in order to avoid the noise generated by the sensor in those bands.

Fig. 16 represents the average spectral signatures of 48 healthy pixel samples and 12 tumour pixel samples and their respective minimum and maximum variances. Like the VNIR spectral signatures, these ones have been obtained after the application of the pre-processing chain without the spectral band reduction and, also the first and last bands have too noise and should be refused. As it can be seen in the chart, the spectral range between 1120 nm to 1400 nm could be of interest for the classification algorithms.
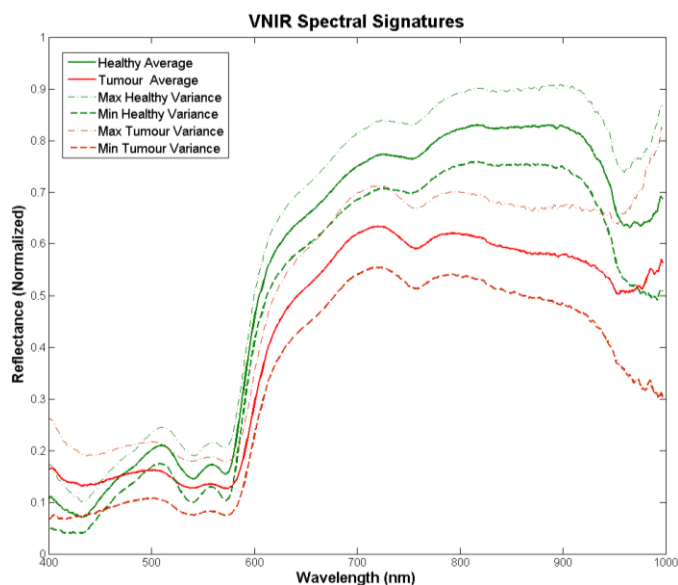

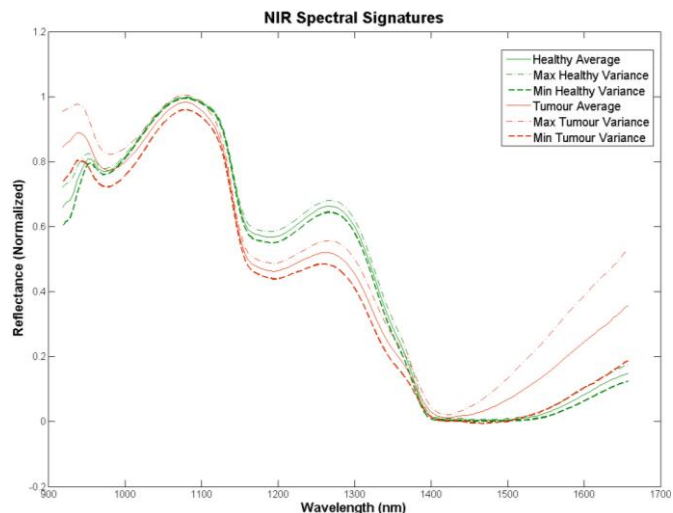Fig. 15. VNIR in-vivo healthy and tumour tissues spectral signatures.

Fig. 16. NIR in-vivo healthy and tumour tissues spectral signatures.

IV. CONCLUSIONS

In this paper it has been described the steps that have been carried out so as to develop a demonstrator for intraoperative brain cancer detection using hyperspectral images within the HELICoiD European project. This demonstrator allows to capture hyperspectral images in the spectral range between 400 nm to 1700 nm, acquiring two hyperspectral data cubes, one in the VNIR range (400 nm to 1000 nm) with 826 spectral bands and one in the NIR range (900 nm to 1700 nm) with 172 spectral bands.

A preliminary hyperspectral image pre-processing chain has been established in order to homogenise the pixel information and reduce the noise and the size of the data to facilitate the computation of the hyperspectral classification algorithms that will be implemented in the high performance processing sub-system platform.

Through a visual analysis of the first in-vivo images acquired in the operating theatre, it can be seen that the processing of the samples with the suitable algorithms could achieve precise results in the discrimination between healthy and tumour tissues. Currently, the on-going works are in the field of the development of the algorithms.

REFERENCES

[1] Fei, B., Akbari, H., & Halig, L. V. (2012). Hyperspectral imaging and spectral-spatial classification for cancer detection. 5th International Conference on BioMedical Engineering and Informatics (BMEI), 62–64. doi:10.1109/BMEI.2012.6513047.

[2] Lu, Guolan. Fei, Baowei. (January 2014). Medical hyperspectral imaging: a review. Journal of Biomedical Optics, 19(1), 010901(1) – 010901(23). doi:10.1117/1.JBO.19.1.010901.

[3] I. Dópido, G. Callicó, D. Bulters, E. Casselden, H. Fabelo and H. Bulstrode. (April 2015). Distinguishing Tumour from Brain using

Machine Classification of Infrared Spectral. Society of British Neurological Surgeons. Southampton, U.K.

[4] Martin, M. E., Wabuyele, M. B., Chen, K., Kasili, P., Panjehpour, M., Phan, M., Overholt, B., Cunningham, G., Wilson, D., DeNovo R.C., & Vo-Dinh, T. (June 2006). Development of an advanced hyperspectral imaging (HSI) system with applications for cancer detection. Annals of Biomedical Engineering, 34(6), 1061–1068. doi:10.1007/s10439-006-9121-9.

[5] Nagaoka, T., Eikje, N. S., Nakamura, A., Aizawa, K., Kiyohara, Y., Ichikawa, F., Yamazaki, T., Doi, M., Nakamaura, K., Otsubo, S.,& Sota, T. (August 2007). Inspection of skin hemodynamics with hyperspectral camera. Proceedings of the 29th Annual International Conference of the IEEE EMBS, 3357–3361. doi:10.1109/IEMBS.2007.4353050.

[6] Jayanthi, J. L., Nisha, G. U., Manju, S., Philip, E. K., Jeemon, P., Baiju, K. V., Beena, V.T., & Subhash, N. (March 2013). Diffuse reflectance spectroscopy: diagnostic accuracy of a non-invasive screening technique for early detection of malignant changes in the oral cavity. BMJ Open, 1, 1–7. doi:10.1136/bmjopen-2011-000071.

[7] Akbari, H., Uto, K., Kosugi, Y., Kojima, K., & Tanaka, N. (April 2011). Cancer detection using infrared hyperspectral imaging. Cancer Science, 102(4), 852–857. doi:10.1111/j.1349-7006. 2011.01849.

[8] Kim, B., Kehtarnavaz, N., Leboulluec, P., Liu, H., Peng, Y., & Euhus, D. (July 2013). Automation of ROI extraction in hyperspectral breast images. 35th Annual International Conference of the IEEE EMBS, 3658–3661. doi:10.1109/EMBC.2013.6610336.

[9] Akbari, H., Kosugi, Y., K., & Tanaka, N. (September 2009). Blood vessel detection and artery-vein differentiation using hyperspectral imaging. 31st Annual International Conference of the IEEE EMBS, 1461–1464. doi:10.1109/IEMBS.2009.5332920.

[10] Akbari, H., Kosugi, Y., Kojima, K., & Tanaka, N. (August 2010). Detection and analysis of the intestinal ischemia using visible and invisible hyperspectral imaging. IEEE Transactions on Biomedical Engineering, 57(8), 2011–2017. doi:10.1109/TBME.2010.2049110.

[11] De Beule, P. A. A., Dunsby, C., Galletly, N. P., Stamp, G. W., Chu, A. C., Anand, U., Anand, P., Benham, C.D., Naylor, A., & French, P. M. W. (December 2007). A hyperspectral fluorescence lifetime probe for skin cancer diagnosis. Review of Scientific Instruments, 78(12), 123101(1)–123101(7). doi:10.1063/1.2818785.

[12] Liu, Z., Wang, H., & Li, Q. (2012). Tongue tumor detection in medical hyperspectral images. Sensors, 12, 162–174. doi:10.3390/s120100162.